nature methods

ARTICLES

https://doi.org/10.1038/s41592-019-0471-2

A genetically encoded fluorescent sensor for in vivo imaging of GABA

Jonathan S. Marvin[1], Yoshiteru Shimoda[2], Vincent Magloire[2], Marco Leite[2], Takashi Kawashima[1], Thomas P. Jensen[2], Ilya Kolb[1], Erika L. Knott[3], Ondrej Novak[1,4], Kaspar Podgorski[1], Nancy J. Leidenheimer[3], Dmitri A. Rusakov[2], Misha B. Ahrens[1], Dimitri M. Kullmann[2] and Loren L. Looger[1*]

Current techniques for monitoring GABA (γ-aminobutyric acid), the primary inhibitory neurotransmitter in vertebrates, cannot follow transients in intact neural circuits. To develop a GABA sensor, we applied the design principles used to create the fluorescent glutamate receptor iGluSnFR. We used a protein derived from a previously unsequenced *Pseudomonas fluorescens* strain and performed structure-guided mutagenesis and library screening to obtain intensity-based GABA sensing fluorescence reporter (iGABASnFR) variants. iGABASnFR is genetically encoded, detects GABA release evoked by electric stimulation of afferent fibers in acute brain slices and produces readily detectable fluorescence increases in vivo in mice and zebrafish. We applied iGABASnFR to track mitochondrial GABA content and its modulation by an anticonvulsant, swimming-evoked, GABA-mediated transmission in zebrafish cerebellum, GABA release events during interictal spikes and seizures in awake mice, and found that GABA-mediated tone decreases during isoflurane anesthesia.

GABA is a ubiquitous inhibitory neurotransmitter, reducing neuronal excitability by receptor-mediated hyperpolarization of membrane potential and shunting of excitatory currents. $GABA_A$ receptors are hetero-pentameric Cl^--conducting channels[1]. $GABA_B$ receptors are hetero-dimeric metabotropic receptors that are coupled to multiple ionic currents by $G_{i/o}$-proteins[2] and are more sensitive to GABA than most synaptic $GABA_A$ receptors[3].

Despite the clinical efficacy of drugs that alter GABAergic neurotransmission, the details of GABA release from neurons remain largely unknown. GABA signaling has traditionally been inferred from a combination of electrophysiology and pharmacology[4]. Direct detection of GABA has required microdialysis followed by derivatization and quantification by HPLC and electrochemistry[5], but this technique has an inherently poor spatiotemporal resolution (on the order of minutes and hundreds of microns).

Although genetically encoded fluorescent sensors for calcium[6–8] have been optimized for imaging neural activity and sensors for the excitatory neurotransmitter glutamate[9] have been developed, methods for directly imaging GABAergic signaling are lacking. A semisynthetic sensor with organic fluorophores attached to the $GABA_B$ receptor was reported[10], but its low affinity for GABA (400 μM) and dependence on two small molecules limit utility. Inhibitory neurotransmission can be inferred from the intracellular chloride concentration, $[Cl^-]_i$, using Clomeleon[11]. However, $[Cl^-]_i$ does not change much during inhibition; the sensors conflate the activities of all ligand-gated (GABA, glycine) and voltage-gated Cl^- channels; and $GABA_B$ receptors are $G_{i/o}$-coupled receptors that do not directly affect $[Cl^-]_i$. Thus, direct detection is preferable for inference of GABAergic signaling in general and is required for mechanistic studies of synaptic input-output transformations, as recently shown with glutamate release and presynaptic Ca^{2+} imaging[12,13].

We have generalized the development of genetically encoded sensors from bacterial periplasmic binding proteins (PBPs) by insertion of circularly permuted fluorescent proteins[14], including a glutamate sensor for in vivo imaging[9]. Here we report the development of an iGABASnFR and observe GABA uptake into mitochondria and GABA release in cultured neurons and acute mouse brain slice. In vivo, we observed bulk GABA transients in mouse visual cortex, and GABA release synchronized with interictal spikes and seizures in a chemoconvulsant mouse model of epilepsy. In zebrafish, we used iGABASnFR to correlate GABAergic signals across the cerebellum to motor output.

Results

Sensor engineering. There are many potential scaffolds for developing a GABA sensor. $GABA_A$ and $GABA_B$ receptors are inappropriate since the GABA binding sites of the former are at protein–protein interfaces[1] (rather than intramolecular) and the latter is difficult to express heterologously[15]. Furthermore, over-expression of these receptors could alter cellular physiology. In theory, one could redesign the binding site of an existing sensor (for example iGluSnFR) to make it specific for GABA. However, our attempts to do so failed (data not shown).

GABA is a prominent signaling molecule in plants. The plant pathogen *Agrobacterium tumefaciens* expresses two periplasmic GABA binding proteins. We developed a sensor from Atu2422 (ref. [16]), but it has low (high-μM) affinity for GABA and orders-of-magnitude higher (low-μM) affinity for alanine and proline (Supplementary Fig. 1). Atu4243 has more stringent specificity and higher affinity for GABA (9 μM)[17]. Unfortunately, Atu4243 with either cpGFP (circularly permuted green fluorescent protein) or cp-superfolder GFP (cpSFGFP) inserted at various locations

[1]Janelia Research Campus, Howard Hughes Medical Institute, Ashburn, VA, USA. [2]UCL Queen Square Institute of Neurology, University College London, London, UK. [3]Louisiana State University Health Sciences Center, Shreveport, LA, USA. [4]Second Medical Faculty, Charles University, Prague, Czech Republic. *e-mail: loogerl@hhmi.org

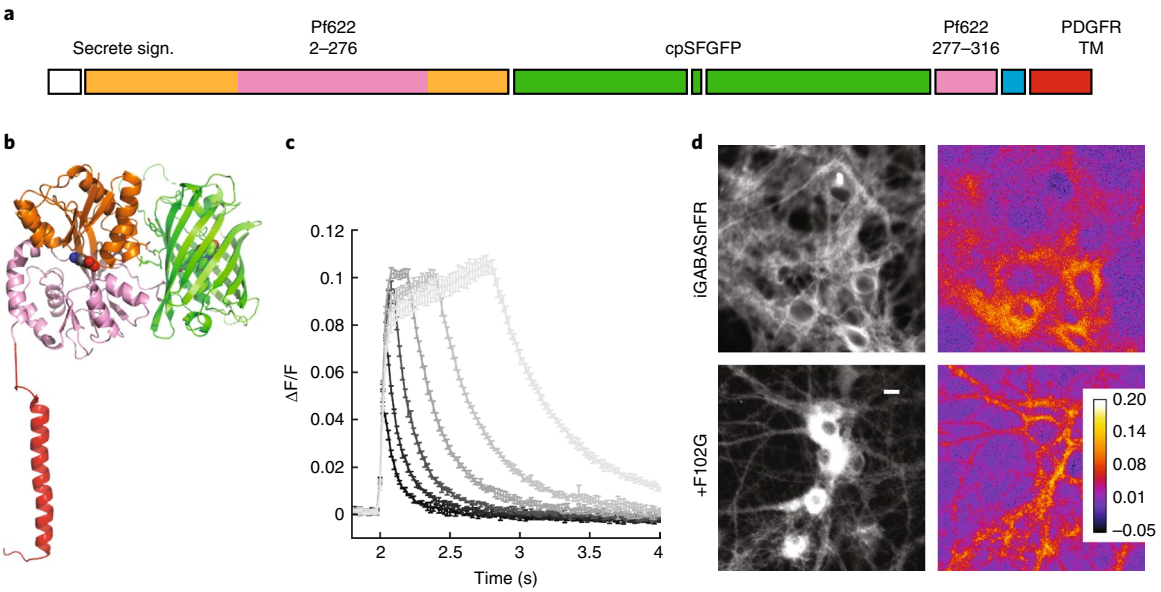

Fig. 1 | Sensor design and characterization in neuronal culture. a, Schematic of the primary sequence. White, IgG secretion signal (which gets cleaved); orange and pink, GABA binding protein Pf622, colored according to domain assignment in **b**; green, cpSFGFP; blue, Myc epitope tag; red, PDGFR transmembrane (TM) domain. **b**, Open unliganded structure of a preliminary version of iGABASnFR. Gray spheres indicate the approximate position of GABA, based on homology to the closed liganded structure of Atu4243. Note that the transmembrane domain is included for illustrative purposes only and was not part of the soluble structure. **c**, Averaged response ($n = 3$ replicates, ±s.d.) of a region of interest (ROI) selected in a region of maximal ΔF/F to multiple stimuli (50 Hz). Black to light gray, 1, 2, 5, 10, 20, 40 field stimuli. **d**, Wide-field fluorescence and fluorescence difference images of iGABASnFR (top) and iGABASnFR.F102G (bottom) expressed in neuronal culture. ΔF/F heat map is shown for the maximum response to ten field stimuli. Scale bar, 20 μm. The response was similar in five repetitions.

did not translocate to the membrane surface in cultured cells (Supplementary Fig. 2) and was abandoned.

Before the structures of Atu2422 and Atu4243 were published, a strain of *Pseudomonas fluorescens* (ATCC no. BAA1781) was reported to take up GABA[18]. We sequenced the genome of this strain (CNG89; a gift from Dr. Catherine Guthrie). We identified 'Pf622' as a homolog of Atu4243 (Supplementary Fig. 3) and expressed it heterologously in *Escherichia coli*. The affinity of the protein was not in the low-nM range as expected[18], but rather ~110 μM as determined by isothermal titration calorimetry (Supplementary Fig. 4). A fluorescent allosteric signal transducer[19], introduced by attaching an environmentally sensitive fluorophore, JF585 (ref. [20]), via maleimide-thiol chemistry to a cysteine mutation at a residue in the hinge of the protein (V278C), resulted in a hybrid sensor with 240 μM affinity for GABA (Supplementary Fig. 5). Stopped-flow analysis revealed atypical kinetics. Instead of a single exponential rise in fluorescence upon the mixing of protein and GABA, the data is best fit by a double exponential (Supplementary Fig. 6a,b), suggesting that multiple steps link GABA binding to fluorescence change (see below). Regardless, the rise time for Pf622.V278C-JF585 binding GABA is longer than it is for iGluSnFR binding glutamate (Supplementary Fig. 6c).

Pf622 with cpGFP or cpSFGFP (whose substitution for cpGFP in iGluSnFR[9] improved expression and photostability) inserted at any of several sites translocated to the membrane when cloned into pDisplay and expressed in mammalian cells (Supplementary Fig. 7). We inserted cpSFGFP after residue 276 of Pf622 (Fig. 1a; Supplementary Fig. 8), optimized binding protein-to-FP linkers, yielding a first-generation sensor (L1-LA/L2-AN), and solved its crystal structure in the unliganded, open state (Fig. 1b, Supplementary Fig. 9, PDB accession 6DGV). The homology of Pf622 to Atu4243, for which both the unliganded, open and bound, closed structures are available[17], allowed us to test mutations to the hinge region of Pf622 expected to allosterically modulate affinity[21]. Hinge mutation F101L increased affinity 10-fold (Supplementary Fig. 10). Mutation of a residue in Pf622 (N260A) that potentially interacted with cpSFGFP, and was also a potential glycosylation site, increased brightness in HEK cells (Supplementary Fig. 11). Re-optimization of the linkers (L1-LAQVR, L2-AN), plus the SFGFP mutation F145W, resulted in a variant, called iGABASnFR, worthy of further characterization. In summary, iGABASnFR is Pf622 with cpSFGFP inserted after residue 276, with optimized linkers (L1-LAQVR, L2-AN), a hinge mutation (F101L), an interface and expression mutation (N260A) and an additional GFP mutation (F145W).

In vitro characterization. Purified iGABASnFR shows a maximum ΔF/F of ~2.5, where $\Delta F/F = (F\text{-}F_0)/F_0$ and F_0 is basal fluorescence, and a dissociation constant (K_d) for GABA of ~9 μM (Supplementary Fig. 12a). It shows no affinity for other amino acids except very low affinity for glycine (500 μM), alanine (830 μM) and histidine (2.4 mM) (Supplementary Fig. 12b). It has no affinity for similar four-carbon metabolites fumarate, malate, oxaloacetate, nor succinate (data not shown). As we characterized iGABASnFR in cellular systems, we made additional efforts to increase its affinity and ΔF/F. Mutation of a GABA-binding pocket residue to its Atu4243 homolog, F102Y, had minimal effect on GABA affinity and decreased ΔF/F. Meanwhile, the mutation Y137L increased ΔF/F, at the cost of poor expression. The double mutant F102Y.Y137L expressed well, exhibited higher ΔF/F (3.5 versus 2.5 for iGABASnFR) but lower affinity (70 μM versus 9 μM for iGABASnFR; Supplementary Fig. 12a). Addition of F102G to iGABASnFR (without changes to Y137) showed higher ΔF/F (4.5) and affinity of 50 μM. We created a non-binding variant by mutating a binding pocket residue (R205A). iGABASnFR and the +F102G and +F102Y.Y137L variants were further characterized.

We profiled the iGABASnFR variants for binding to GABAergic drugs (Supplementary Fig. 12c-f). Baclofen (β-(4-chlorophenyl)-GABA) affected all three iGABASnFR variants tested (as well as

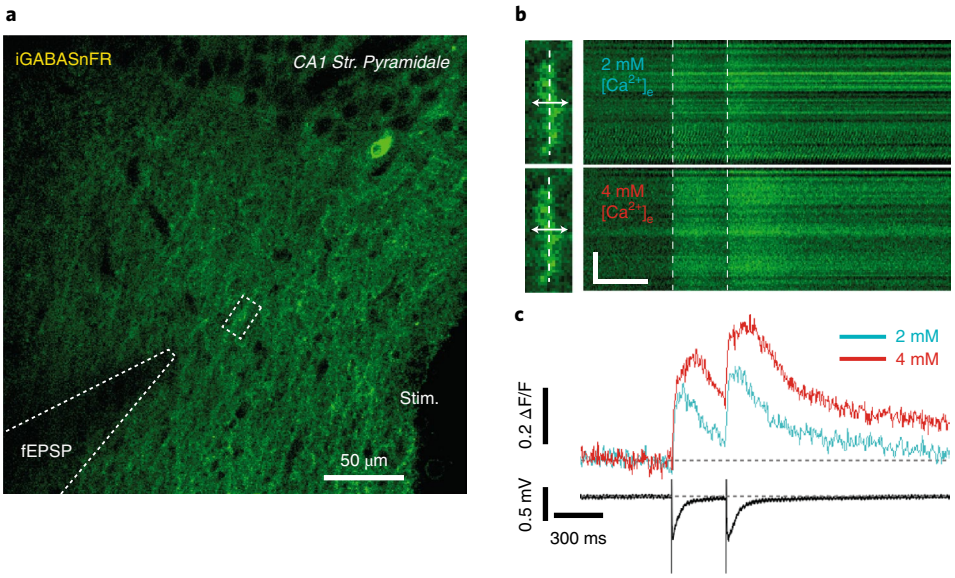

Fig. 2 | Recording of stimulus-evoked extracellular GABA transients using iGABASnFR transfected acute brain slices. a, Experimental setup: concentric bipolar stimulation electrode (stim.) placed in hippocampal CA1 *stratum radiatum*. Paired pulse stimulation (200 µs pulse width) was given with a 300 ms interstimulus interval (1st stimulation at 2 s). At the same time, the field EPSP was recorded in proximity to the imaging ROI and used to calibrate the stimulation amplitude (half-maximal). The segment, arising from the green cell visible in *stratum pyramidale*, was scanned under two-photon excitation (910 nm) using a frame scan across a dendrite of interest (ROI; white box in **a**). **b**, Left, enlarged image of ROI. Center line and arrows indicate region for *x* axis integration for linescan images. Right, Mean linescan of ten stimulation trials recorded with a 30 s interval in 2 mM extracellular [Ca^{2+}] (top) and 4 mM [Ca^{2+}] (bottom). Dashed lines indicate the onset of extracellular stimulation. Extracellular Ca^{2+} concentration was raised to increase presynaptic GABA release probability. **c**, Overlaid iGABASnFR response averages. Blue, 2 mM Ca^{2+}; red, 4 mM Ca^{2+}. Black line represents a concurrently recorded field EPSP (fEPSP). Mean $n = 10$ trials.

the negative control cpSFGFP, Supplementary Fig. 12c), whereas vigabatrin (γ-vinyl-GABA, Sabril) bound to only iGABASnFR. F102G. All three variants are also high-affinity sensors for muscimol (Supplementary Fig. 12c-f, pink traces). Importantly, all other drugs showed much weaker binding to the sensors than GABA, allowing them to be used in conjunction with iGABASnFR imaging. The absorbance, excitation and emission profiles of iGABASnFR show that fluorescence changes result from increased excitation at 485 nm when GABA is bound, and is reflected in the two-photon cross sections of all three iGABASnFR variants (Supplementary Fig. 13). The iGABASnFR variants are more sensitive to pH in the unbound state than the GABA-bound state (Supplementary Fig. 14). Unlike other PBP-based sensors[9,21], the rate of fluorescence change for iGABASnFR as determined by stopped-flow kinetics was largely independent of the concentration of ligand used (Supplementary Fig. 15).

GABA processing in mitochondria. After being transported into mitochondria (by an as yet unidentified transporter), GABA is degraded by GABA transaminase (GABA-T). Inhibition of GABA-T elevates synaptic levels of GABA[22] and, of clinical significance, the GABA-T inhibitor vigabatrin is a prescribed antiepileptic[23]. We transfected cultured prostate cancer cells (LNCaP) with iGABASnFR. F102Y.Y137L (which does not bind vigabatrin; Supplementary Fig. 12f), fused to an N-terminal mitochondrial matrix targeting motif from Cox8a (mito-iGABASnFR.F102Y.Y137L). Basal fluorescence was low (Supplementary Fig. 16), consistent with the observation that these cells contain little GABA[24]. Exogenous GABA increased fluorescence within the mitochondria as expected (Supplementary Fig. 17a,b), reaching equilibrium after 48 h, presumably reflecting both increasing mito-iGABASnFR expression and continued GABA uptake. The GABA-binding dependence of mitochondria-localized iGABASnFR is hyperbolic (Supplementary Fig. 17c). Vigabatrin treatment tends to increase iGABASnFR fluorescence in mitochondria (Supplementary Fig. 17d). Transfection of mito-iGABASnFR. F102Y.Y137L expressing LNCaP cells with a plasmid encoding glutamic acid decarboxylase 1 (*GAD67*) resulted in increased endogenous GABA synthesis (Supplementary Fig. 17e).

Neuronal culture characterization. iGABASnFR variants cloned into a modified version of pDisplay lacking the HA tag expressed in HEK cells and showed good membrane localization (Supplementary Fig. 11). Similarly, iGABASnFR showed good membrane localization and brightness at 14 d in vitro (DIV) in primary culture of hippocampal neurons from P0 newborn rats after infection with AAV2/1. *hSynapsin1*.iGABASnFR, but the +F102G and +F102Y.Y137L variants were noticeably dimmer and showed intracellular accumulation (Supplementary Fig. 18). Perfusion of neuronal cultures with GABA revealed affinities for GABA similar to, but slightly weaker than, purified protein (iGABASnFR, 30 µM; +F102G, 42 µM; +F102Y.Y137L, 106 µM; Supplementary Fig. 19).

Electrical field stimulation (50 Hz) of the cultured neurons produced fluorescence changes from single stimulus-evoked action potentials and increased until plateauing after 40 stimuli (Fig. 1c). The fluorescence change of iGABASnFR was restricted to the membrane (Fig. 1d), as with SF-iGluSnFR, but with an order of magnitude lower maximal response (Supplementary Fig. 20a). The iGABASnFR response within a field of view was also less uniform than SF-iGluSnFR (Supplementary Fig. 20b–e), consistent with GABAergic neurons representing a smaller fraction (~10%) of the neuronal population in the hippocampal culture[25].

Hippocampal acute slice. To confirm that iGABASnFR remains functional in brain tissue, we examined hippocampal acute slices prepared from mice injected with AAV2/1.*hSynapsin1*.iGABASnFR. Although it was challenging to reliably record GABA release at individual synapses (data not shown), which was possible for glutamate recording with iGluSnFR[12,13], iGABASnFR displayed excellent signal-to-noise ratio following paired pulse extracellular field

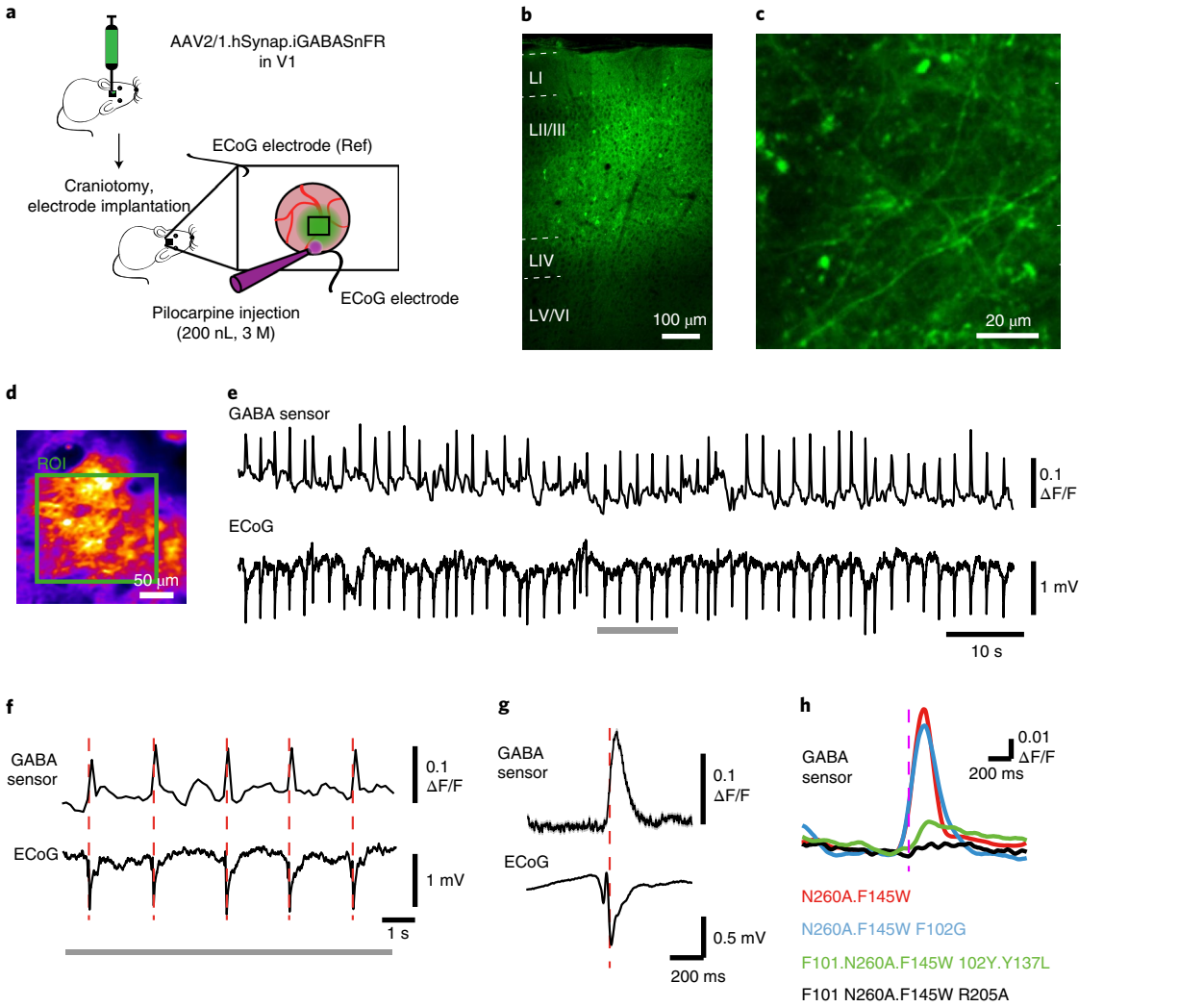

Fig. 3 | iGABASnFR response during interictal spiking. a, Experimental design. Ref, reference electrode. **b**, iGABASnFR expression in transduced area imaged after the end of the experiment, using immunofluorescence microscopy. Scale bar, 100 µm. Cortical layers (layers I, II/III, IV, and V/VI) are shown. **c**, iGABASnFR expression in vivo in cortical neuron processes 100 µm below the pia. Scale bar, 20 µm. **d**, Average iGABASnFR fluorescence image during interictal activity. Scale bar, 50 µm. **e**,**f**, Simultaneous fluorescence (averaged in green square in **d**) and interictal ECoG. Gray bar indicates the enlargement window in **f**. **g**, Time-course of iGABASnFR fluorescence and interictal ECoG averaged from 68 events in one experiment. **h**, Comparison of average fluorescence transients obtained with different sensors. Similar results were observed in two additional animals.

stimulation in *stratum radiatum*. iGABASnFR responses to extracellular GABA transients were recorded from apical dendritic segments traced from the CA1 pyramidal cell body (Fig. 2a). Raising extracellular calcium increased fluorescence response amplitude (Fig. 2b,c), consistent with increased presynaptic release probability[26].

Somatosensory cortex acute slice. We also probed the effect of iGABASnFR expression on post-synaptic signaling. Since the sensor is derived from a bacterial binding protein, it is unlikely to interact with $GABA_A$ or $GABA_B$ receptors. In acute brain slices of mouse somatosensory cortex, whole-cell patch-clamp recordings of uninfected and AAV.*hSynapsin1*.iGABASnFR infected cells showed resting potentials near the expected −70 mV (Supplementary Fig. 21a). Patched cells were observed for 100 s with inhibitory and excitatory post-synaptic currents (IPSCs and EPSCs) electrically stimulated every 10 s. Evoked excitatory current from cells expressing iGABASnFR were statistically indistinguishable from uninfected cells (Supplementary Fig. 21b,c; $P=0.63$ for evoked EPSC peak currents; $P=0.35$ for evoked IPSC peak currents; Mann–Whitney *U*-test). Spontaneous post-synaptic currents (PSCs) were observed in the intervening periods (Supplementary Fig. 21d). The amplitudes of these spontaneous PSCs were similar (spontaneous mean amplitude for EPSCs, $P=0.97$; IPSCs, $P=0.82$; Supplementary Fig. 21e), as were the amplitude variances (spontaneous amplitude s.d. for EPSCs, $P=0.92$; IPSCs, $P=0.92$; Mann–Whitney *U*-test; Supplementary Fig. 21f). Evoked responses measure purely post-synaptic activity, while spontaneous activity is also influenced by differences in network connectivity and inputs, which vary from cell to cell. So, although we observed a higher (but statistically insignificant) frequency of spontaneous IPSCs in iGABASnFR-expressing cells (0.19 Hz versus 0.12 Hz, $P=0.066$; Mann–Whitney *U*-test; Supplementary Fig. 21g), the absence of other differences between iGABASnFR infected and uninfected cells leads us to believe that the observed higher frequency of IPSCs in iGABASnFR cells is coincidental.

Volume detection of GABA in mouse visual cortex. In the visual cortex, GABAergic inhibition[27] and disinhibition[28] contribute to context-dependent processing and can enhance the distinctness of sensory responses. Hypnotic effects of anesthetics have been

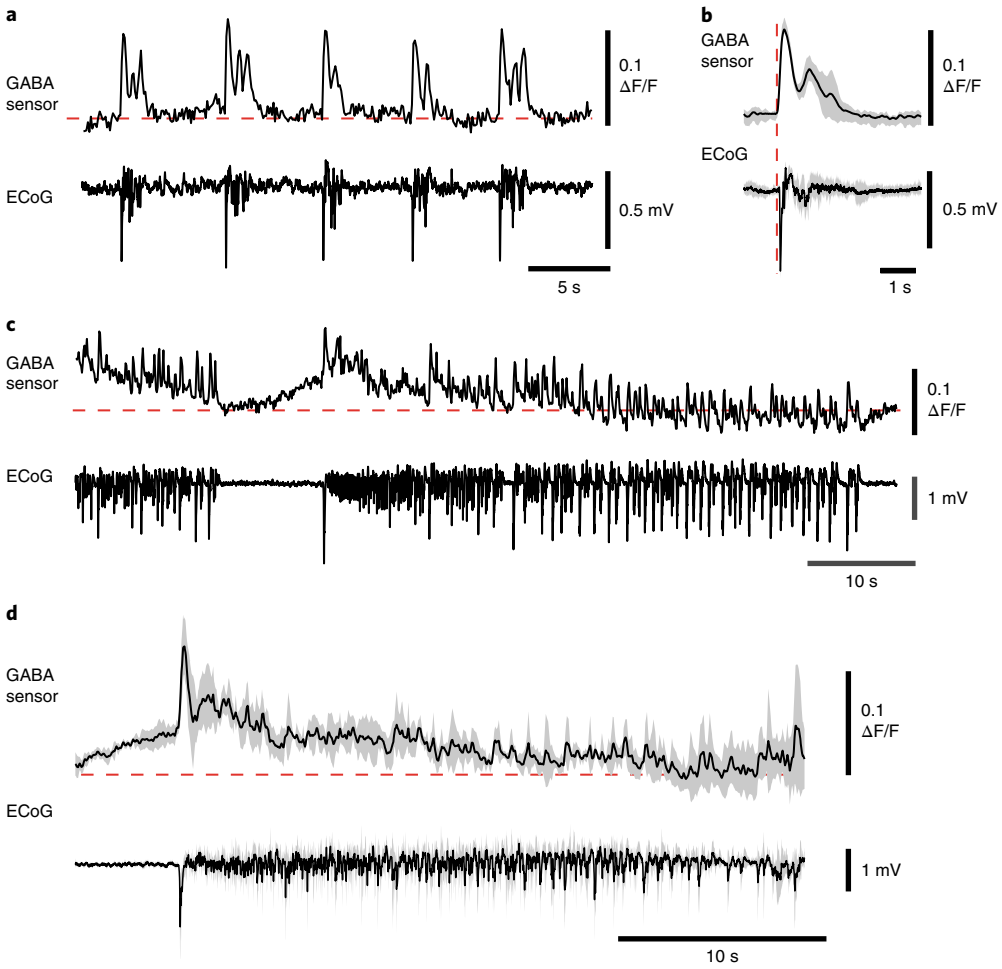

Fig. 4 | GABA sensor behavior during polyspikes and seizures. a, Trains of polyspikes (ECoG, bottom) evoked by pilocarpine and simultaneous iGABASnFR.F102G fluorescence (top). Similar results were observed in two additional animals. **b**, Average time-course of sensor fluorescence and ECoG during polyspike (mean ± s.d. indicated as shaded area from five seizures in one animal). **c**, iGABASnFR.F102G fluorescence during seizures. Note that the envelope of the fluorescence transients gradually decreases during seizures (monoexponential decay time constant ~12.1 s) and then slowly recovers during periods of electrographic silence before the return of seizure activity (monoexponential time constant ~16.0 s). This is a single observation due to the sporadic nature of seizures. **d**, Average (black line) time-course of sensor fluorescence and ECoG during seizures (mean of four seizures, ±s.d. indicated as shaded area).

associated with GABAergic transmission[29]. Volatile anesthetics decrease both glutamatergic and GABAergic synaptic transmission in the cortex, with stronger effects on glutamate currents, leading to net inhibition of activity[30]. Anesthetics can, therefore, be used to determine whether iGABASnFR can detect decreases in cortical GABA release relative to basal rates, which may reflect tonic[31] or ongoing phasic release.

To directly monitor cortical GABA in a time- and depth-resolved manner, we injected AAV2/1.*hSynapsin1*.iGABASnFR into mouse primary visual cortex (V1) and measured fluorescence (with 1030 nm excitation) in a 150 × 150 × 450 μm^3 deep volume over the course of 40 min. After 8 min, we administered isoflurane anesthesia, which is expected to suppress inhibition. Fluorescence decreased 20% during anesthesia treatment and slowly returned to baseline during recovery (Supplementary Fig. 22a,b). In parallel experiments with the non-GABA-binding negative control (R205A), fluorescence decayed slowly over the observation period, with no recovery after removal of anesthesia (Supplementary Fig. 22c).

In vivo mouse model of epilepsy. Having established that iGABASnFR robustly detects synchronous release events, we tested it in small-scale, high-resolution, two-photon neuropil imaging experiments. Focal neocortical epilepsy is typically accompanied by abnormal background electrocorticogram (ECoG) activity, including frequent interictal spikes (occurring between seizures), which are dominated by GABAergic activity[32]. How seizures intermittently arise from this background is poorly understood. Numerous mechanisms have been proposed, although the strongest evidence supports a failure of feed-forward inhibition[33,34]. This could, in principle, arise because interneurons enter a state of depolarization block in the face of over-excitation and fail to release GABA, or because shifts in the chloride reversal potential in principal cells resulting from intense GABA release render $GABA_A$ receptor-mediated inhibition ineffective[35]. These hypotheses are not mutually exclusive, but important insights could be provided by imaging extracellular GABA during interictal spiking and seizures. If extracellular GABA transients collapse rapidly at the onset of seizures, this would argue for depolarization block of interneurons, or another mechanism by which interneurons fail to be recruited or release GABA.

We injected AAV2/1.*hSynapsin1*.iGABASnFR (or variants) into layer 2/3 of mouse V1 (Fig. 3a–d). Intracortical pilocarpine injection elicited focal epileptiform activity lasting up to 60 min[36]. This consisted of periods of interictal spiking alternating with polyspikes and ECoG seizures lasting 1–2 min. iGABASnFR

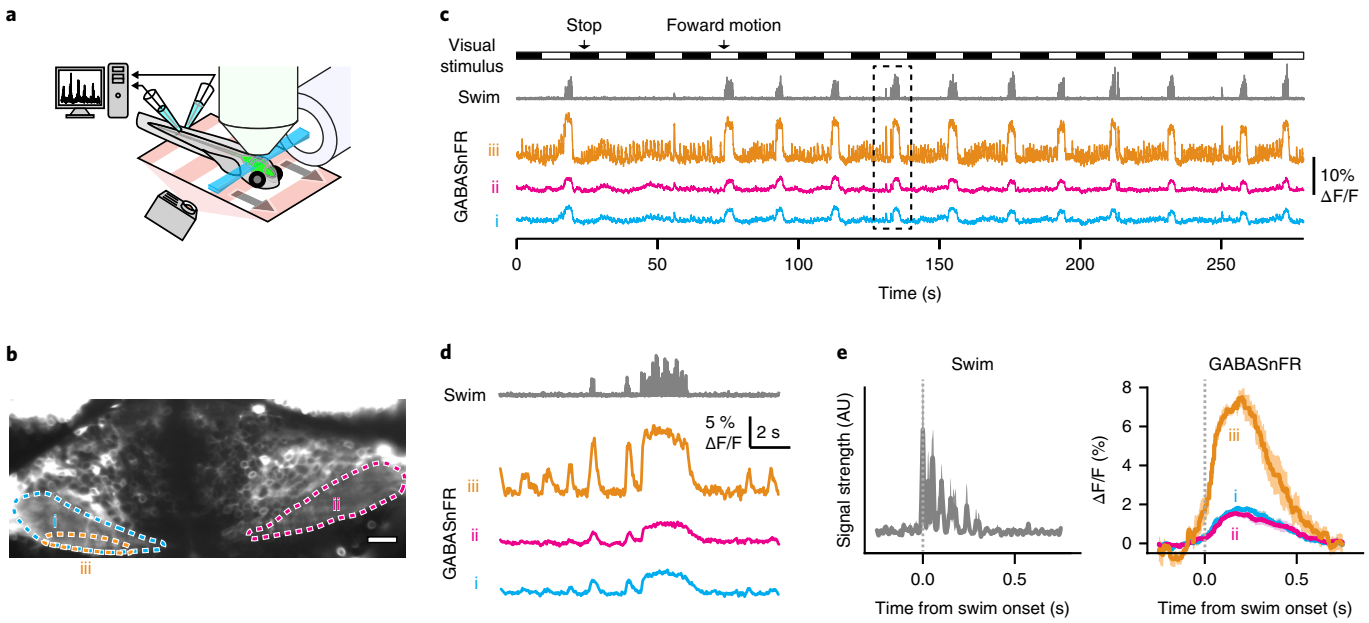

Fig. 5 | GABA response measured with iGABASnFR.F102Y.Y137L fluorescence in a fictive model of swimming in zebrafish larvae. See also Supplementary Video 1, in which changes in fluorescence within region (iii) are visible. **a**, Schematic illustration of the setup. An immobilized zebrafish is placed under the light-sheet microscope and the fictive motor signals from its tail are recorded during the imaging session. Visual stimuli below the fish move forward (arrows) to induce swimming. **b**, Light-sheet image of zebrafish cerebellum expressing iGABASnFR.F102Y.Y137L under the *elavl3* promoter. Three regions of interest (i, ii, iii) within the neuropil (excluding cerebellar cell bodies) are indicated by dotted lines. Bright, clipped regions at the top are optic tectum. **c**,**d**, Forward motion of visual stimuli (white boxes), fictive motor signals (gray) and fluorescent signals from regions of interest indicated in **b**. Traces in the dotted box in **c** are expanded in **d**. **e**, Motor signals (left) and fluorescence changes (right) averaged across five swim events. Shadows represent s.e.m. across swim events. Data shown are from a single fish.

fluorescence reliably showed transients time-locked to interictal spikes (Fig. 3e-g). Comparing across the different sensors, iGABASnFR and iGABASnFR.F102G gave the largest ΔF/F, iGABASnFR.F102Y.Y137L gave lower ΔF/F and iGABASnFR.R205A was unresponsive (Fig. 3h).

During periods with stereotyped polyspikes, fluorescence peaks separated by <1 s could be resolved with iGABASnFR.F102G (Fig. 4a,b). Discrete peaks coinciding with low-frequency ECoG components could still be seen during focal seizures lasting up to 1 min (Fig. 4c). Fluorescence gradually decreased during seizures, slowly recovering during intervals of electrographic silence between seizures (Fig. 4c,d). As this slow decrease was not seen during interictal events and polyspikes (Fig. 3e and Fig. 4a,b), it cannot be attributed to photobleaching. It is, however, consistent with iGABASnFR acidification (Supplementary Fig. 14). Extracellular acidification during seizures has been documented abundantly and has been proposed to contribute to seizure termination[37]. The decrease in fluorescence (starting 1 s after the onset of the seizure, Fig. 4d) yielded a monoexponential decay time constant of approximately 12.1 s, similar to the time constant for pH changes in astrocytes during seizures (~14.7 s, ref. [38]). Fluorescence increased during periods of electrographic silence between seizures, consistent with pH return-to-baseline. (A monoexponential curve fit from the end of one seizure to the start of the next (average time interval around 8.2 s) yielded a time constant around 16 s). Although this account of changes in fluorescence is consistent with a surge in GABA and changes in extracellular pH, further experiments using a GABA-insensitive pH indicator, such as pHluorin, or an improved pH-insensitive GABA sensor, would help to distinguish the two phenomena.

GABA in zebrafish cerebellum. As a final demonstration of iGABASnFR in vivo, we observed GABA transients in *Danio rerio* (zebrafish) cerebellum using light-sheet imaging in a fictive model of swimming[39] (Fig. 5a). In zebrafish, fictive swimming triggers robust activation of GABAergic cerebellar Purkinje cells[40]. We generated a transgenic zebrafish expressing iGABASnFR.F102Y.Y137L (available before iGABASnFR.F102G was identified) under the *elavl3*/*HuC* pan-neuronal promoter (Fig. 5b). During swim bouts, we observed reliable fluorescence changes in cerebellar neuropil regions containing GABAergic Purkinje cell axons[41] (Fig. 5c,d, Supplementary Video 1). Changes in fluorescence peaked roughly 200 ms after the onset of swimming (Fig. 5e), with this region producing >8% fluorescence increases. This result indicates that iGABASnFR can reliably detect local GABA transmission that may play a critical role in motor control.

Discussion

To understand neural circuit function, numerous specific inputs onto neurons must be disentangled from their integrated output. Current sensor technologies, namely SF-iGluSnFR[9], GCaMP6 (ref. [7]) and jGCaMP7 (ref. [8]) and jRGECO[6], are sensitive enough to allow reliable detection of excitatory synaptic transmission, excitatory post-synaptic currents and action potentials. Indicators for inhibitory synaptic transmission and inhibitory post-synaptic currents have lagged far behind. iGABASnFR offers the best performance of existing GABA indicators and is the only one to be genetically encoded completely, facilitating in vivo use. Calcium and glutamate sensors have been iteratively optimized, both to improve overall performance and to match the precise requirements of specific settings. We expect further development of iGABASnFR, with altered affinity and kinetics and improved signal-to-noise ratio. Different colors of iGABASnFR could also be developed, allowing simultaneous imaging in orthogonal chromatic channels, as has been done with iGluSnFR[9,42]. More sensitive indicators will be required to facilitate single-spine GABAergic imaging and the separation of phasic from tonic signaling.

It is important to note the value of spatially resolvable readout of synaptic GABA release given the highly organized, cell type-specific nature of GABAergic innervation onto pyramidal cells[43]. Imaging in different cellular compartments enables the high-throughput study of GABA release from different populations of interneurons. Combined with patch-clamp electrophysiology and Ca^{2+} imaging with red-shifted indicators, iGABASnFR could allow direct study of the local signaling requirements underlying important physiological phenomena such as depolarization-induced inhibition suppression[44].

In our data, GABA release does not collapse completely during seizures. However, our experiments do not rule out the partial failure of GABA release when seizures start, due either to exhaustion of releasable GABA vesicles or to depolarization block in a subset of interneurons. Indeed, we imaged very superficial cortex, restricting the observation of GABA release to pyramidal neuron dendrites and layer 1 interneurons. Ultimately, to understand the role of GABA during seizures, more extensive experiments involving different interneuron types, simultaneous glutamate imaging and controlling for pH is needed.

We hope that the demonstrated use of iGABASnFR in models of epilepsy and in the cerebellum of fictively behaving zebrafish will help elucidate the role of GABA in various circuits, during development and in disease states. Aberrations in GABAergic signaling occur in Alzheimer's disease[45], Parkinson's[46], Huntington's[47], schizophrenia[48], autism[49] and Rett syndrome[49]. The imaging of iGABASnFR in appropriate animal models will facilitate a greater understanding of these mechanisms. iGABASnFR could also allow easy screening of candidate transporters such as the vertebrate mitochondrial GABA transporter. Applications outside neuroscience are also possible, such as separating the critical roles of GABA in plant metabolism and signaling.

Online content

Any methods, additional references, Nature Research reporting summaries, source data, statements of code and data availability and associated accession codes are available at https://doi.org/10.1038/s41592-019-0471-2.

Received: 15 May 2018; Accepted: 28 May 2019;
Published online: 15 July 2019

References

1. Fritschy, J.-M. & Panzanelli, P. $GABA_A$ receptors and plasticity of inhibitory neurotransmission in the central nervous system. *Eur. J. Neurosci.* **39**, 1845–1865 (2014).
2. Padgett, C. L. & Slesinger, P. A. $GABA_B$ receptor coupling to G-proteins and ion channels. *Adv. Pharm* **58**, 123–147 (2010).
3. Sodickson, D. L. & Bean, B. P. $GABA_B$ receptor-activated inwardly rectifying potassium current in dissociated hippocampal CA3 neurons. *J. Neurosci.* **16**, 6374–6385 (1996).
4. Macdonald, R. L. & Olsen, R. W. $GABA_A$ receptor channels. *Annu. Rev. Neurosci.* **17**, 569–602 (1994).
5. van der Zeyden, M., Oldenziel, W. H., Rea, K., Cremers, T. I. & Westerink, B. H. Microdialysis of GABA and glutamate: analysis, interpretation and comparison with microsensors. *Pharmacol. Biochem. Behav.* **90**, 135–147 (2008).
6. Dana, H. et al. Sensitive red protein calcium indicators for imaging neural activity. *eLife* **5**, 413 (2016).
7. Chen, T.-W. et al. Ultrasensitive fluorescent proteins for imaging neuronal activity. *Nature* **499**, 295–300 (2013).
8. Dana, H. et al. High-performance GFP-based calcium indicators for imaging activity in neuronal populations and microcompartments. *Nat. Methods* https://doi.org/10.1038/s41592-019-0435-6 (2019).
9. Marvin, J. S. et al. Stability, affinity, and chromatic variants of the glutamate sensor iGluSnFR. *Nat. Methods* **15**, 936–939 (2018).
10. Masharina, A., Reymond, L., Maurel, D., Umezawa, K. & Johnsson, K. A fluorescent sensor for GABA and synthetic $GABA_B$ receptor ligands. *J. Am. Chem. Soc.* **134**, 19026–19034 (2012).
11. Grimley, J. S. et al. Visualization of synaptic inhibition with an optogenetic sensor developed by cell-free protein engineering automation. *J. Neurosci.* **33**, 16297–16309 (2013).
12. Jensen, T. P., Zheng, K., Tyurikova, O., Reynolds, J. P. & Rusakov, D. A. Monitoring single-synapse glutamate release and presynaptic calcium concentration in organised brain tissue. *Cell Calcium* **64**, 102–108 (2017).
13. Jensen, T. P. et al. Multiplex imaging relates quantal glutamate release to presynaptic Ca^{2+} homeostasis at multiple synapses in situ. *Nat. Commun.* **10**, 1414–1414 (2019).
14. Marvin, J. S., Schreiter, E. R., Echevarría, I. M. & Looger, L. L. A genetically encoded, high-signal-to-noise maltose sensor. *Proteins* **79**, 3025–3036 (2011).
15. Geng, Y. et al. Structure and functional interaction of the extracellular domain of human GABA(B) receptor GBR2. *Nat. Neurosci.* **15**, 970–978 (2012).
16. Planamente, S. et al. A conserved mechanism of GABA binding and antagonism is revealed by structure-function analysis of the periplasmic binding protein Atu2422 in Agrobacterium tumefaciens. *J. Biol. Chem.* **285**, 30294–30303 (2010).
17. Planamente, S. et al. Structural basis for selective GABA binding in bacterial pathogens. *Mol. Microbiol.* **86**, 1085–1099 (2012).
18. Guthrie, G. D. & Nicholson-Guthrie, C. S. Gamma-Aminobutyric acid uptake by a bacterial system with neurotransmitter binding characteristics. *Proc. Natl Acad. Sci. USA* **86**, 7378–7381 (1989).
19. Marvin, J. S. et al. The rational design of allosteric interactions in a monomeric protein and its applications to the construction of biosensors. *Proc. Natl Acad. Sci. USA* **94**, 4366–4371 (1997).
20. Grimm, J. B. et al. A general method to fine-tune fluorophores for live-cell and in vivo imaging. *Nat. Methods* **14**, 987–994 (2017).
21. Marvin, J. S. & Hellinga, H. W. Manipulation of ligand binding affinity by exploitation of conformational coupling. *Nat. Struct. Biol.* **8**, 795–798 (2001).
22. Engel, D. et al. Plasticity of rat central inhibitory synapses through GABA metabolism. *J. Physiol.* **535**, 473–482 (2001).
23. Brunton, L., Chabner, B. & Knollman, B. *Goodman and Gilman's The Pharmacological Basis of Therapeutics* 12th edn (McGraw Hill Professional, 2011).
24. Putluri, N. et al. Metabolomic profiling reveals a role for androgen in activating amino acid metabolism and methylation in prostate cancer cells. *PLoS ONE* **6**, e21417 (2011).
25. Benson, D. L., Watkins, F. H., Steward, O. & Banker, G. Characterization of GABAergic neurons in hippocampal cell cultures. *J. Neurocytol.* **23**, 279–295 (1994).
26. Dodge, F. A. & Rahamimoff, R. Co-operative action of calcium ions in transmitter release at the neuromuscular junction. *J. Physiol.* **193**, 419–432 (1967).
27. Adesnik, H., Bruns, W., Taniguchi, H., Huang, Z. J. & Scanziani, M. A neural circuit for spatial summation in visual cortex. *Nature* **490**, 226–231 (2012).
28. Zhang, S. et al. Selective attention. Long-range and local circuits for top-down modulation of visual cortex processing. *Science* **345**, 660–665 (2014).
29. Nelson, L. E. et al. The sedative component of anesthesia is mediated by GABA(A) receptors in an endogenous sleep pathway. *Nat. Neurosci.* **5**, 979–984 (2002).
30. Westphalen, R. I. & Hemmings, H. C. Selective depression by general anesthetics of glutamate versus GABA release from isolated cortical nerve terminals. *J. Pharmacol. Exp. Ther.* **304**, 1188–1196 (2003).
31. Farrant, M. & Nusser, Z. Variations on an inhibitory theme: phasic and tonic activation of GABA(A) receptors. *Nat. Rev. Neurosci.* **6**, 215–229 (2005).
32. Cohen, I., Navarro, V., Clemenceau, S., Baulac, M. & Miles, R. On the origin of interictal activity in human temporal lobe epilepsy in vitro. *Science* **298**, 1418–1421 (2002).
33. Trevelyan, A. J., Sussillo, D. & Yuste, R. Feedforward inhibition contributes to the control of epileptiform propagation speed. *J. Neurosci.* **27**, 3383–3387 (2007).
34. Schevon, C. A. et al. Evidence of an inhibitory restraint of seizure activity in humans. *Nat. Commun.* **3**, 1060 (2012).
35. Magloire, V., Mercier, M. S., Kullmann, D. M. & Pavlov, I. GABAergic interneurons in seizures: investigating causality with optogenetics. *Neuroscientist* https://doi.org/10.1177/1073858418805002 (2018).
36. Kätzel, D., Nicholson, E., Schorge, S., Walker, M. C. & Kullmann, D. M. Chemical-genetic attenuation of focal neocortical seizures. *Nat. Commun.* **5**, 3847 (2014).
37. Ziemann, A. E. et al. Seizure termination by acidosis depends on ASIC1a. *Nat. Neurosci.* **11**, 816–822 (2008).
38. Raimondo, J. V. et al. Tight coupling of astrocyte pH dynamics to epileptiform activity revealed by genetically encoded pH sensors. *J. Neurosci.* **36**, 7002–7013 (2016).
39. Ahrens, M. B. et al. Brain-wide neuronal dynamics during motor adaptation in zebrafish. *Nature* **485**, 471–477 (2012).
40. Scalise, K., Shimizu, T., Hibi, M. & Sawtell, N. B. Responses of cerebellar Purkinje cells during fictive optomotor behavior in larval zebrafish. *J. Neurophysiol.* **116**, 2067–2080 (2016).
41. Tanabe, K. et al. Atypical protein kinase C regulates primary dendrite specification of cerebellar Purkinje cells by localizing Golgi apparatus. *J. Neurosci.* **30**, 16983–16992 (2010).

42. Wu, J. et al. Genetically encoded glutamate indicators with altered color and topology. *ACS Chem. Biol.* **13**, 1832–1837 (2018).
43. Somogyi, P. & Klausberger, T. Defined types of cortical interneurone structure space and spike timing in the hippocampus. *J. Physiol.* **562**, 9–26 (2005).
44. Ohno-Shosaku, T. et al. Presynaptic cannabinoid sensitivity is a major determinant of depolarization-induced retrograde suppression at hippocampal synapses. *J. Neurosci.* **22**, 3864–3872 (2002).
45. Jo, S. et al. GABA from reactive astrocytes impairs memory in mouse models of Alzheimer's disease. *Nat. Med* **20**, 886–896 (2014).
46. Emir, U. E., Tuite, P. J. & Öz, G. Elevated pontine and putamenal GABA levels in mild-moderate Parkinson disease detected by 7 Tesla proton MRS. *PLoS ONE* **7**, e30918 (2012).
47. Raymond, L. A. et al. Pathophysiology of Huntington's disease: time-dependent alterations in synaptic and receptor function. *Neuroscience* **198**, 252–273 (2011).
48. Simpson, M. D., Slater, P., Deakin, J. F., Royston, M. C. & Skan, W. J. Reduced GABA uptake sites in the temporal lobe in schizophrenia. *Neurosci. Lett.* **107**, 211–215 (1989).
49. Chao, H.-T. et al. Dysfunction in GABA signalling mediates autism-like stereotypies and Rett syndrome phenotypes. *Nature* **468**, 263–269 (2010).

Acknowledgements

We would like to thank Catherine S. Nicholson-Guthrie (Indiana University) for the gift of the *Pseudomonas fluorescens* strain CNG89; D. Stern, S. Picard, A. Lemire and D. Kao for helping sequence the genome of CNG89; D.Walpita for rat neuronal culture; J. Macklin and R. Patel for collecting two-photon spectra; and A. Abdelfattah and C.-L. Hsu for assistance with brain slice recordings. Y.S., M.L. and D.M.K. are supported by the Medical Research Council (grant no. MR/L01095X/1) and Wellcome Trust (grant nos. 095580/Z/11/Z and 212285/Z/18/Z). V.M. is supported by Epilepsy Research UK (grant no. P1702). T.P.J. and D.A.R. are supported by the Wellcome Trust Principal Fellowship (no. 212251/Z/18/Z) and European Research Council Advanced Grant (no. 323113). M.A. is supported by Simons Collaboration on the Global Brain Research Awards 325171 and 542943SPI. This work was supported by the Howard Hughes Medical Institute.

Author contributions

J.S.M. and L.L.L. were responsible for protein engineering and experimental design and led the project. T.P.J. and D.A.R. performed hippocampal slice imaging. I.K. was responsible for somatosensory slice electrophysiology. K.P. and O.N. performed visual cortex volume imaging. Y.S., V.M., M.L. and D.M.K. produced the mouse epilepsy model. E.L.K. and N.J.L performed mitochondrial experiments. T.K. and M.B.A. designed and performed the zebrafish experiments.

Competing interests

The authors declare no competing interests.

Additional information

Supplementary information is available for this paper at https://doi.org/10.1038/s41592-019-0471-2.

Correspondence and requests for materials should be addressed to L.L.L.

Peer review information: Nina Vogt was the primary editor on this article and managed its editorial process and peer review in collaboration with the rest of the editorial team.

Methods

Sequencing of the Pseudomonas fluorescens strain CNG89 genome. Genomic DNA was prepared using a QIAamp DNA mini kit (Qiagen). Genomic DNA was sequenced using a combination of Ion Torrent PGM and Illumina HiSeq technologies and assembled using Spades software with default parameters. Draft genome assembly (131 scaffolds; 141,337 base pairs median scaffold length, N_{50}) was sufficient to facilitate tblastn of the *Agrobacterium tumefaciens* Atu4243 sequence to prioritize putative GABA-binding proteins. The complete genome assembly is ongoing and will be published elsewhere.

Cloning and mutagenesis. The gene for Pf622, lacking the periplasmic leader sequence, was amplified by PCR and cloned into pRSET-A (Invitrogen) by BamHI and EcoRI digest. Silent mutations were made to remove an internal PstI restriction site. The Pf622 gene was then re-cloned into a derivative of pRSET that has the N-terminal affinity and epitope tags replaced by an Arg-Ser encoding BglII site and a C-terminal Leu-Gln-His_6 sequence (with PstI encoding Leu-Gln). This pRSET derivative was created to facilitate downstream cloning of iGABASnFR variants into AAV vectors. Genes for Pf622-cpSFGFP insertions were made by overlapping PCR.

Mutant screening. Mutations to iGABASnFR variants were made by the uracil template-based method[50]. Mutations were initially targeted to the junction of Pf622 and cpSFGFP and expanded to include other residues as the sensor was improved. Mutated plasmids were transformed into T7 express cells (New England BioLabs), plated on Luria broth agar plates with 100 μg ml^{-1} ampicillin and grown overnight at 37 °C. Colonies were transferred to 2 ml 96-well plates containing 0.9 ml auto-induction media[51] with 100 μg ml^{-1} ampicillin and grown overnight with vigorous shaking (400 r.p.m.) at 30 °C. Bacterial pellets were collected by centrifugation (3000*g*), resuspended in 0.5 ml PBS by vortexing to wash away endogenous GABA and then pelleted again. The wash procedure was repeated five times, and pellets were frozen overnight at −20 °C. Frozen bacterial pellets were then lysed by the addition of 1 ml PBS and vortexing. Cellular debris was pelleted by centrifugation and clarified lysate removed for fluorescence assays by pipetting.

The green fluorescence (excitation 485 nm, emission 515 nm, 5 nm bandpass) of 100 μl clarified lysate was measured in a Tecan Infinite M1000 Pro plate-reading fluorimeter. GABA was added to a final concentration of 1 mM and fluorescence was measured again. Variants with increased ΔF/F over the starting construct were immediately re-assayed to estimate binding affinity, and the best were streaked out on agar plates, re-isolated, re-assayed and sequenced.

Protein expression, purification and in vitro characterization. Final variants of iGABASnFR were expressed as above, but on a larger scale (0.5 l) and pelleted by centrifugation, resuspended in PBS and frozen overnight. Cells were lysed by thawing and sonication. Lysate was clarified by centrifugation at 35,000*g* and purification by immobilized metal affinity chromatography on a 5 ml fast flow chelating sepharose column (GE Life Sciences) with an elution gradient from 0 to 200 mM imidazole over 120 ml. Fluorescent fractions were pooled, concentrated by spin concentrator and dialyzed five times in PBS. Equilibrium binding affinities were determined by titration with serial dilutions of GABA (or other compounds) into 0.2 μM protein solution in PBS. Kinetics of binding were determined by mixing equal volumes of 0.2 μM protein with varying concentrations of GABA in an Applied Photophysics SX20 stopped-flow fluorimeter with 490 nm LED excitation and 510 nm long pass filter. Circular dichroism was measured with 20 μM protein in 0.1× PBS in an Applied Photophysics Chirascan with 1 s data collection periods and 300 s settling time at each temperature point. Two-photon cross sections were collected for 1 μM solutions of protein in PBS with or without 10 mM GABA, excited by pulses from a mode-locked Ti:Sapphire laser (Chameleon Ultra, Coherent, 80 MHz, 140-fs pulse width, 1 mW power at the focus). Emission was detected by an avalanche photodiode (PDM Series, Micro Photon Devices) with a 550 nm filter (88-nm bandpass).

Prostate cell measurements. LNCaP cells were seeded in each well of a 96-well plate at a density of 25,000 cells per well in triplicate for each condition. Fluorescence was quantified by the IncuCyte ZOOM live-cell imaging microscope system (Sartorius) and analyzed using IncuCyte ZOOM 2016B edition software. Four fields of view, predetermined by the software, were imaged for each well of the 96-well plate, every 4 h. The total object integrated intensity values were compiled for each well at each time point. No ROIs were selected; instead, collected fields were quantified in their entirety. To determine total object integrated intensity values, cells were analyzed by the 'top hat' background subtraction algorithm to subtract non-uniform background (Essen BioScience, IncuCyte Background Fluorescence Technical Note). Radius values for fluorescence masking were calibrated to 1.3× the radius of the largest cell-associated fluorescent object in the representative image set. Fluorescence (arbitrary units) values of images from control wells (that is, untreated iGABASnFR transfected for GABA/vigabatrin experiments; iGABASnFR + empty vector transfected for GAD1 experiments) were thresholded to display a fluorescent object count of zero at the time of the first scan. The above analysis parameters were applied across all images within an experiment. Fluorescence values for transfection controls (empty vector, that is, no mito-iGABASnFR) were less than 0.1% but were nevertheless subtracted at each time point for the corresponding treatment conditions.

Primary rat hippocampal neuron cultures. All animal procedures were approved by the Institutional Animal Care and Use and Institutional Biosafety Committees at the HHMI Janelia Research Campus. A mixed cell culture (neurons and glia) was prepared from Sprague Dawley rat pups (Charles River Laboratories). Briefly, P0 pups (either sex) were decapitated and the brains were dissected into ice-cold neural dissection solution (10 mM HEPES, Sigma, in HBSS, Invitrogen, pH 7.4). Cortical tissue was dissected and cut into small pieces to facilitate enzyme digestion. Cortex pieces were transferred using a large bore pipette into a 15 ml conical tube and incubated with enzyme digest solution (Papain, Worthington Biologicals) at 37 °C for 30 min. After 30 min, the enzyme solution was removed and plating media (MEM media containing 10% fetal bovine serum) was added and tissue pieces were triturated resulting in mostly single cells. The cell suspension was filtered using a 45 μm filter. The filtered cell suspension was centrifuged, and the resulting cell pellet was resuspended with plating media and counted. Cells were plated onto coverslips coated with poly-D-lysine (Sigma) and kept at 37 °C, 5% CO_2 in Plating Media. For viral infection, 1 μl of 10^{13} genomic copies per milliliter (GC ml^{-1}) was diluted into NbActiv4 and added on DIV3, with 50% of the media exchanged for fresh media every 4 d.

Imaging was performed on DIV14. Growth media was replaced with an imaging buffer containing 10 mM HEPES, 145 mM NaCl, 2.5 mM KCl, 10 mM D-glucose, 2 mM $CaCl_2$, 1 mM $MgCl_2$, pH 7.4. Images were collected on a Nikon Eclipse Ti2 wide-field fluorescence microscope with a Plan Apo ×20 0.75 numerical aperture objective. Fluorescence was excited with a 470 nm LED and emission collected through a 525 nm (36 nm bandpass) filter. Images were collected at 50 Hz. Field stimulation was achieved with a WPI stimulus isolator, 1 ms, 90 mA, 50 Hz, platinum bar electrodes held in place with a bespoke holder.

Hippocampal slices. All animal procedures were conducted in accordance with the European Commission Directive (86/609/EEC) and the United Kingdom Home Office (Scientific Procedures) Act (1986). Young C57BL/6J mice (Envigo, 3–4 weeks of age) male and female, were anaesthetized using isoflurane (5% induction, 1.5–2.5% v/v). Upon loss of pedal withdrawal reflexes, the animal was secured in a stereotaxic frame (David Kopf Instruments). Perioperative analgesics were administered (subcutaneous buprenorphine, 60 μg kg^{-1}) and the scalp was shaved and disinfected using three washes of topical chlorhexidine. A small midline incision was made and the skull was exposed. A craniotomy was performed over the right hemisphere using a high-speed hand drill (Proxxon) equipped with a 0.4 mm circular drill burr. The location overlaid the medial hippocampus (Stereotactic coordinates were 60% of the anterio–posterior distance from Bregma to lambda and 2.5 mm lateral to midline). Once exposed, a warmed artificial cerebrospinal fluid (aCSF) variant (cortex buffer; 125 mM NaCl, 5 mM KCl, 10 mM HEPES, 10 mM glucose, 2 mM $CaCl_2$, 2 mM $MgSO_4$) was applied to the skull and cortical surface throughout the procedure.

Pressure injections of AAV2/1.*hSynapsin*.iGABASnFR (totaling 0.1–1 × 10^{10} genomic copies in a volume not exceeding 200 nl) were carried out using a pulled glass micropipette stereotactically guided to a depth of 1.3 mm beneath the cortical surface, at a rate of approximately 1 nl s^{-1}. The total injection volume was delivered in three steps, reducing depth by 100 μm at each step. Once delivery was completed, pipettes were left in place for 5 min before being retracted. The surgical wound was closed with absorbable 7-0 sutures (Ethicon Endo-Surgery GmbH) and the animal was left to recover in a heated chamber. Meloxicam (subcutaneous, 1 mg kg^{-1}) was subsequently administered once daily for up to 2 d following surgery. Mice were killed by transcardial perfusion with ice-cold sucrose-enriched slicing medium (105 mM sucrose, 60 mM NaCl, 2.5 mM KCl, 1.25 mM NaH_2PO_4, 26 mM $NaHCO_3$, 15 mM glucose, 1.3 mM ascorbic acid, 3 mM Na pyruvate, 0.5 mM $CaCl_2$ and 7 mM $MgCl_2$, saturated with 95% O_2 and 5% CO_2). After a 2–4 week incubation period, acute hippocampal slices were prepared for imaging and electrophysiological recordings as below.

Acute 350 μm thick hippocampal slices were obtained from 5–7-week-old C57BL/6J mice (Envigo), as specified, in full compliance with national guidelines on animal experimentation. Slices were prepared in an ice-cold slicing solution described below, stored in the slicing solution at 34 °C for 15 min before being transferred to a submersion chamber for storage in an extracellular solution containing 119 mM NaCl, 2.5 mM KCl, 1.3 mM $MgSO_4$, 1 mM NaH_2PO_4, 26 mM $NaHCO_3$, 2 mM $CaCl_2$, 10 mM glucose (osmolarity adjusted to 295–305 mOsM with glucose). All solutions were continuously bubbled with 95% O_2 and 5% CO_2. Slices were allowed to rest for at least 60 min before recordings started.

For imaging of evoked GABA transients, we used a Femtonics Femto3D-RC imaging system, integrated with patch-clamp electrophysiology (Femtonics) and linked on the same light path to two femtosecond pulse lasers MaiTai (SpectraPhysics-Newport) with independent shutter and intensity control as previously described[12,13]. Cells were first identified as iGABASnFR-expressing using two-photon imaging at 910 nm and dendrites were followed from the CA1 pyramidal cell soma into *stratum radiatum*. Once a suitable dendritic segment was found a concentric bipolar stimulating electrode was lowered into position

~100 microns distant on the axis of the Schaffer collaterals in *stratum radiatum*. Dendritic iGABASnFR responses were recorded with a frame scanning ROI placed over a dendritic segment. Scans of 3.5 s duration were made at a sampling frequency of ~200 Hz with 2P excitation at 910 nm. During recording iGABASnFR responses were evoked by paired 100 µs constant-current electrical stimulation of an amplitude that evoked a ~50% maximal field EPSP; recorded through a locally placed 1.5–2 MΩ resistance glass electrode filled with aCSF. Recorded scan data were analyzed using Femtonics MES and traces expressed as ΔF/F.

Brain slice electrophysiology. All animal procedures were approved by the Institutional Animal Care and Use and Institutional Biosafety Committees at the HHMI Janelia Research Campus. Mice of either sex ($n = 4$, C57BL/6J, Charles River, 4 weeks old) were bilaterally injected in the primary somatosensory cortex (1.2 mm posterior, 2.25 mm lateral, relative to Bregma) with 40 nl of AAV2/1.*hSynapsin1*.iGABASnFR (10^{13} GC ml^{-1}) at two depths (300 and 600 µm).

After 2–4 weeks, mice were deeply anesthetized with isoflurane, and the brain was quickly removed and transferred to an ice-cold sucrose solution containing 150 mM Sucrose, 40 mM NaCl, 4 mM KCl, 1.25 mM $NaH_2PO_4 \cdot H_2O$, 7 mM $MgCl_2$, 25 mM $NaHCO_3$, 10 mM D-Glucose, 0.5 mM $CaCl_2 \cdot 2H_2O$ (pH 7.3–7.4, 300–310 mOsm). Coronal brain slices were cut (300 µm thick) with a vibrating tissue slicer (VT 1200 S, Leica Microsystems) and subsequently incubated at 37 °C for 1 h in recording solution consisting of 124 mM NaCl, 2.5 mM KCl, 1.25 mM NaH_2PO_4, 1.3 mM $MgCl_2$, 26 mM $NaHCO_3$, 10 mM D-Glucose, 2 mM $CaCl_2 \cdot 2H_2O$, 1 mM Na-Ascorbate (pH 7.3-7.4, 290–300 mOsm). The sucrose and recording solutions were constantly bubbled with 95% O_2 and 5% CO_2. Slices were then transferred to a custom-machined recording chamber, perfused with room-temperature recording solution and held down with a slice anchor (SHD-41/10, Warner Instruments).

Cells expressing iGABASnFR were identified on an upright epifluorescent microscope (Olympus BX-51 WI) equipped with an LED illumination system (470 nm, pE-2, CoolLED). Whole-cell voltage clamp recordings were performed with a Multiclamp 700b (Molecular Devices) amplifier. Patch-clamp pipettes were pulled on a horizontal puller (P-97, Sutter Instruments) to a tip resistance of 4 to 8 MΩ and filled with internal solution containing: 115 mM Cs-methanesulfonate, 15 mM CsCl, 3.5 mM Mg-ATP, 5 mM NaF, 10 mM EGTA, 10 mM HEPES, 3 mM QX-315 (pH: 7.3–7.4, 280–290 mOsm). For membrane voltage measurements in current clamp, we used 130 mM K-methanesulfonate, 1 mM $MgCl_2$, 1 mM Mg-ATP, 5 mM NaCl, 1 mM Na-ATP, 10 mM HEPES, 14 mM Phosphocreatine (pH: 7.3–7.4, 280–290 mOsm). Synaptic responses were evoked with short square pulses (0.1 ms duration, 10 s interstimulation interval) delivered to a bipolar stimulating electrode (TM33CCNON, World Precision Instruments) through a stimulus isolator (A365, World Precision Instruments). Pulse amplitude was set such that single evoked PSCs were reliably excited with minimum current (range 0.3–0.6 mA). Series resistance was compensated at least 60%. Evoked EPSCs were recorded while holding the cell at −70 mV and IPSCs at 0 mV. Ten stimulus responses were recorded and averaged for each cell.

Spontaneously occurring excitatory and inhibitory PSCs were analyzed in recording segments between stimulation pulses. The PSC peak times were manually identified, and amplitude was determined by subtracting the recording baseline averaged over the 10–50 ms time period before the PSC. Only PSCs with amplitudes >20 pA were considered sufficiently distinct from recording noise (~10 pA, peak). PSC frequency was determined by counting the number of spontaneously occurring PSCs per 100 s observation window.

Statistical significance was computed using unpaired Mann–Whitney *U*-test. Statistics were computed using Prism (GraphPad).

Anesthesia. All animal procedures were approved by the Institutional Animal Care and Use and Institutional Biosafety Committees at the HHMI Janelia Research Campus. *Parvalbumin*-T2A-Cre mice (females, 6–8 weeks at the time of the surgery, Jax no. 012358) and *VGAT*-IRES-Cre mice (males, 8–12 weeks at the time of the surgery, Jax no. 028862) were anesthetized using isoflurane in oxygen (3–4% for induction, 1.5–2% for maintenance), placed on a 37 °C heated pad and subcutaneously administered buprenorphine HCl (0.1 mg kg^{-1}) and ketoprofen (5 mg kg^{-1}). Each mouse's head was gently restrained by a toothbar (David Kopf 923-B). A flap of skin and underlying tissue covering the parietal bones and the intraparietal bone was removed. The sutures of the frontal and parietal bones were covered with a thin layer of cyanoacrylate glue. A ring-shaped titanium headbar was glued over the left parietal cortex. We carefully drilled a ~4.5 mm craniotomy (centered in the middle of the left parietal bone) using a high-speed microdrill (Osada, EXL-M40). The dura mater was left intact. Glass capillaries (Drummond Scientific, 3-000-203-G/X) were pulled and beveled (30° angle, 20 µm outer diameter). Using a precision injector (Drummond Scientific, Nanoject III) we injected AAV2/1.*hSynapsin1*.iGABASnFR virus (30 nl, 5E11 GC ml^{-1}, 1 nl s^{-1}, 300 µm deep) into 6–8 positions within the left visual cortex. The craniotomy was closed with a 4 mm round no. 1 cover glass and sealed with cyanoacrylate glue. Animals were imaged 5–15 weeks after surgery.

Volumetric raster two-photon imaging was performed, using a piezo objective mount to perform a 400 µm axial scan in 10 µm increments (volume period 12.05 s). Anesthesia (1.5% isoflurane v/v) was initiated at the onset of frame 40 (8 min) and stopped at the onset of frame 120 (24 min). Basal fluorescence F_0 was calculated by averaging the image intensity over the period prior to anesthesia onset, for each depth.

Seizure model. All animal procedures were conducted in accordance with the European Commission Directive (86/609/ EEC) and the United Kingdom Home Office (Scientific Procedures) Act (1986). Male C57BL/6J mice (from Harlan, 7–8-week-old) were anesthetized with isoflurane (5% induction, 1.5–2.5% v/v) and mounted in a stereotaxic frame (Kopf Instruments). Injection of 200 nl (100 nl min^{-1}) of AAV2/1.*hSynapsin1*.iGABASnFR variants (titer > 10^{13} GC ml^{-1}, except for F102G variant 6×10^{12} GC ml^{-1}) into layer 2/3 of primary visual cortex (Antero-posterior: −2.8 mm from Bregma and Lateral: 2.4 mm, depth: 0.3 mm below the pia) was performed using a microinjection pump (WPI Ltd.), a 5 µl Hamilton syringe and a 33-gauge needle (Esslab Ltd.). Two to three weeks later, a craniotomy was performed over the visual cortex and electrocorticogram (ECoG) electrodes and a head-plate (Neurotar) were implanted under isoflurane anesthesia. After recovery, the mice were trained to tolerate brief sessions of immobilization via the head-plate. On the day of the experiment, pilocarpine (3.5 M, 0.2–0.3 µl) was injected into layer 5 (approximately 1–2 mm from the imaging area, depth 0.5 mm) close to the region of interest. Imaging was performed with a FV1200MPE multi-photon laser scanning microscope (Olympus), coupled to a Chameleon Ultra pulsed laser (Coherent, wavelength 908 nm). The ECoG was acquired via a MultiClamp 700B amplifier (Molecular Devices), time-stamped with the imaging data. ECoG data were bandpass-filtered from 0.1 to 300 Hz and digitized at 1 kHz. The imaging frame rate was typically 10 Hz, and the region of interest was up to 0.25×0.25 mm^2. For the data shown here the fluorescence was averaged across the entire region of interest, or where iGABASnFR was expressed. To average the time-course of the GABA fluorescence transient occurring during interictal spiking, a shift and mean algorithm[52] was applied to blocks of frames straddling each spike.

Transgenic zebrafish. All animal procedures were approved by the Institutional Animal Care and Use Committee at the HHMI Janelia Research Campus. Transgenic zebrafish expressing iGABASnFR were generated as follows. A sequence of iGABASnFR.F102Y.Y137L was cloned downstream of the *HuC/elavl3* promoter[53]. This plasmid was injected into two-cell stage embryos of *Casper* mutant zebrafish[54] with mRNA of Tol2 transposase[55] to generate founder (F0) transgenic zebrafish.

Imaging experiments were performed using 5-d old embryos. The zebrafish were immobilized and mounted to an imaging chamber as described previously[53]. Briefly, the muscles of the zebrafish were paralyzed by a short (up to 30 seconds) bath incubation with alpha-bungarotoxin (1 mg ml^{-1}, Thermo Fischer Scientific, B1601) dissolved in external solution. After the fish became immobile, the zebrafish were further mounted to a custom-made chamber using 2% agarose (Sigma-Aldrich, A9414) and placed under a light-sheet microscope with a ×16 objective lens (Nikon, CFI75 LWD ×16 W). Imaging was performed using a 488 nm laser (180 µW) and a 525/50 emission filter (Semrock, FF03-525/50) with a frame rate of 30 frames s^{-1}.

To record swim signals from the axonal bundles of spinal motoneurons in the tail, we attached a pair of large barrel electrodes to the dorsal left and right sides of the tail. Signals were amplified by an amplifier (Molecular Devices, AxoClamp 700B) and recorded at 6 kHz using custom software written in C# (Microsoft). For synchronization between the swim signals and neural activity images, camera trigger signals that initiate the acquisition of individual frames in the light-sheet microscope were simultaneously recorded with the swim signals. During the experiments, we projected red visual stimuli (red or black gratings with bars 2 mm thick) onto the bottom of the fish chamber. The speed of the moving visual stimulus alternated between 0 mm s^{-1} (stopped) and 2 mm s^{-1} (moving forward) every 10 s. This forward movement of visual stimulus reliably triggered swimming (Fig. 5c).

Statistical tests. Data are presented as the mean with s.e.m. or s.d., as noted in each case. All values of *n* are provided; no data were excluded. For comparisons between two datasets, a two-sided Student's *t*-test was used, unless specified otherwise.

Reporting Summary. Further information on research design is available in the Nature Research Reporting Summary linked to this article.

Data availability

All data from this study are available upon request. All constructs have been deposited at Addgene (112159–112180). Sequences have been deposited in GenBank(MH392466, MH392467 and MH392468). Protein structure has been uploaded to the Protein Data Bank (6DGV). AAV virus is available from Addgene.

Code availability

All analysis code used in this study is available upon request.

References

50. Kunkel, T. A., Bebenek, K. & McClary, J. Efficient site-directed mutagenesis using uracil-containing DNA. *Meth. Enzym.* **204**, 125–139 (1991).
51. Studier, F. W. Protein production by auto-induction in high density shaking cultures. *Protein Expr. Purif.* **41**, 207–234 (2005).
52. Rama, S. Shift and mean algorithm for functional imaging with high spatio-temporal resolution. *Front. Cell. Neurosci.* **9**, 446 (2015).
53. Vladimirov, N. et al. Light-sheet functional imaging in fictively behaving zebrafish. *Nat. Methods* **11**, 883–884 (2014).
54. White, R. M. et al. Transparent adult zebrafish as a tool for in vivo transplantation analysis. *Cell Stem Cell* **2**, 183–189 (2008).
55. Kawakami, K. et al. A transposon-mediated gene trap approach identifies developmentally regulated genes in zebrafish. *Dev. Cell* **7**, 133–144 (2004).

nature research

Corresponding author(s): Loren L Looger

Last updated by author(s): May 24, 2019

Reporting Summary

Nature Research wishes to improve the reproducibility of the work that we publish. This form provides structure for consistency and transparency in reporting. For further information on Nature Research policies, see Authors & Referees and the Editorial Policy Checklist.

Statistics

For all statistical analyses, confirm that the following items are present in the figure legend, table legend, main text, or Methods section.

n/a	Confirmed	
☐	☒	The exact sample size (*n*) for each experimental group/condition, given as a discrete number and unit of measurement
☐	☒	A statement on whether measurements were taken from distinct samples or whether the same sample was measured repeatedly
☐	☒	The statistical test(s) used AND whether they are one- or two-sided *Only common tests should be described solely by name; describe more complex techniques in the Methods section.*
☒	☐	A description of all covariates tested
☒	☐	A description of any assumptions or corrections, such as tests of normality and adjustment for multiple comparisons
☐	☒	A full description of the statistical parameters including central tendency (e.g. means) or other basic estimates (e.g. regression coefficient) AND variation (e.g. standard deviation) or associated estimates of uncertainty (e.g. confidence intervals)
☒	☐	For null hypothesis testing, the test statistic (e.g. *F*, *t*, *r*) with confidence intervals, effect sizes, degrees of freedom and *P* value noted *Give P values as exact values whenever suitable.*
☒	☐	For Bayesian analysis, information on the choice of priors and Markov chain Monte Carlo settings
☒	☐	For hierarchical and complex designs, identification of the appropriate level for tests and full reporting of outcomes
☒	☐	Estimates of effect sizes (e.g. Cohen's *d*, Pearson's *r*), indicating how they were calculated

Our web collection on statistics for biologists contains articles on many of the points above.

Software and code

Policy information about availability of computer code

Data collection	LNCaP fluorescence was collected and quantified with IncuCyte ZOOM 2016B. Neuronal culture fluorescence was collected with Nikon NIS Elements V4.60. Hippocampal slice fluorescence was collected and analyzed with Femtonics MES software v5. Cortical slice electrophysiology was collected with a multiclamp 700b amplifier (Molecular Devices) and digitized with a PCI-6321 data aquisition board (National Instruments). Volumetric raster imaging in the anaesthesia experiments was collected with custom software. Electrophysiology from cortical seizures was collected with a Multi Clamp 700b amplifier.
Data analysis	Data was averaged and presented with Microsoft Excel 2016, Kaleidagraph4.5.2, MATLAB_R2014b. Images analysis used ScanImage 2018 and ImageJ 2.0.0-RC-54/1.51h. We used SPAdes-3.11.1-Linux, Origin 6, IncuCyte ZOOM 2016B, WaveSurfer 0.967 and C# 6.0.

For manuscripts utilizing custom algorithms or software that are central to the research but not yet described in published literature, software must be made available to editors/reviewers. We strongly encourage code deposition in a community repository (e.g. GitHub). See the Nature Research guidelines for submitting code & software for further information.

Data

Policy information about availability of data

All manuscripts must include a data availability statement. This statement should provide the following information, where applicable:

- Accession codes, unique identifiers, or web links for publicly available datasets
- A list of figures that have associated raw data
- A description of any restrictions on data availability

All data from this study are available upon request. All constructs have been deposited at Addgene (#112159-112180). Sequences have been deposited in Genbank (MH392466-8). AAV is available form Addgene and upon request.

Field-specific reporting

Please select the one below that is the best fit for your research. If you are not sure, read the appropriate sections before making your selection.

☒ Life sciences ☐ Behavioural & social sciences ☐ Ecological, evolutionary & environmental sciences

For a reference copy of the document with all sections, see nature.com/documents/nr-reporting-summary-flat.pdf

Life sciences study design

All studies must disclose on these points even when the disclosure is negative.

Sample size	No statistical methods were used to determine sample size. Experiments were performed enough times to achieve consistent results and permit statistical analysis when appropriate.
Data exclusions	No data points were excluded.
Replication	No attempts at replication failed. All experiments are shown. All experiments were repeated at least twice.
Randomization	Randomization is not relevant to this study because no comparisons between experimental groups or treatments were made.
Blinding	No blinding was performed because these experiments were performed to optimize and characterize a molecular toolset, not test a hypothesis.

Reporting for specific materials, systems and methods

We require information from authors about some types of materials, experimental systems and methods used in many studies. Here, indicate whether each material, system or method listed is relevant to your study. If you are not sure if a list item applies to your research, read the appropriate section before selecting a response.

Materials & experimental systems

n/a	Involved in the study
☒	☐ Antibodies
☐	☒ Eukaryotic cell lines
☒	☐ Palaeontology
☐	☒ Animals and other organisms
☒	☐ Human research participants
☒	☐ Clinical data

Methods

n/a	Involved in the study
☒	☐ ChIP-seq
☒	☐ Flow cytometry
☒	☐ MRI-based neuroimaging

Eukaryotic cell lines

Policy information about cell lines

Cell line source(s)	LNCaP cells were acquired from ATCC. HEK293 cells were acquired from ATCC for the production of AAV.
Authentication	These cell lines are acquired directly from ATCC. None of the cell lines were authenticated.
Mycoplasma contamination	Cell lines were routinely checked to ensure authenticity and absence of mycoplasma infection. All tested negative.
Commonly misidentified lines (See ICLAC register)	No commonly misidentified cell lines were used.

Animals and other organisms

Policy information about studies involving animals; ARRIVE guidelines recommended for reporting animal research

Laboratory animals	Neuronal cultures were prepared from Sprague-Dawley rat pups (Charles River Laboratories; P0 pups, either sex). Brain slices were prepared from C57BL/6J mice (2 - 4 weeks of age, either sex). Anaesthesia experiments were performed on Parvalbumin-T2A-Cre mice (females, 6-8 weeks at the time of the surgery, Jax #012358) and VGAT-IRES-Cre mice (males, 8-12 weeks at the time of the surgery, Jax #028862). Seizure models was performed on male C57BL/6J mice (from Harlan, UK, 7-8-week-old). Transgenic zebrafish (5 dpf, sex not yet genetically determined) were generated and maintained in-house.
Wild animals	The study did not use wild animals.

Field-collected samples	The study did not involve samples collected from the field.
Ethics oversight	All experiments involving animals were conducted with the oversight of each co-author's home institution. At Janelia (JSM, TK, IK, ON,KP, MBA) were approved by the Janelia Institutional Animal Care and Use and Institutional Biosafety Committees. At UCL (YS, VM, ML, TPJ, DAR, DMK) All animal procedures were conducted in accordance with the European Commission Directive (86/609/ EEC) and the United Kingdom Home Office (Scientific Procedures) Act (1986).

Note that full information on the approval of the study protocol must also be provided in the manuscript.